Available online at www.sciencedirect.com
SCIENCE DIRECT®
International Journal of Heat and Mass Transfer 48 (2005) 5563–5579
International Journal of HEAT and MASS TRANSFER
www.elsevier.com/locate/ijhmt

A two-phase flow pattern map for annular channels under a DC applied voltage and the application to electrohydrodynamic convective boiling analysis

J. Cotton [a,b,*], A.J. Robinson [c], M. Shoukri [a], J.S. Chang [d]

[a] McMaster University, Department of Mechanical Engineering, Hamilton, Ont., Canada, L8S 4L8
[b] Dana Corporation, Thermal Products, Long Manufacturing Division, 656 Kerr Street, Oakville, Ont., Canada, L6K 3E4
[c] Trinity College Dublin, Department of Mechanical and Manufacturing Engineering, Dublin 2, Ireland
[d] McMaster University, Department of Engineering Physics, Hamilton, Ont., Canada, L8S 4L8

Received 7 October 2004; received in revised form 26 May 2005
Available online 29 September 2005

Abstract

An experimental study of tube side boiling heat transfer of HFC-134a has been conducted in a single-pass, counter-current flow heat exchanger under an electric field. By applying 0–8 kV to a concentric inner electrode, the mechanics of EHD induced flow and heat transfer augmentation/suppression have been investigated for flow conditions with inlet qualities of 0% to 60%, mass fluxes from 100 kg/m^2 s to 500 kg/m^2 s, and heat flux levels between 10 kW/m^2 and 20 kW/m^2. A theoretical Steiner type two-phase flow pattern map for flow boiling in the annular channel under applied DC high voltage is also developed. The flow regimes encountered in the convective boiling process have been reconstructed experimentally and compared with the proposed EHD flow regime map. The results show that when the proposed dimensionless criterion $M_d \sim Re^2$ is satisfied, EHD interfacial forces have a strong influence on the flow pattern which is considered to be the primary mechanism affecting the increase in pressure drop and the augmentation or even suppression of heat transfer.

Keywords: Two-phase flow; Electrohydrodynamics (EHD); Convective boiling heat transfer; Flow pattern map

1. Introduction

In order to respond to the demands for more efficient and compact heat exchangers the automotive, space, aircraft, and refrigeration industries must continuously seek out new methods to improve heat exchanger performance. As a result, numerous methods have been conceived and implemented to increase heat transfer coefficients in heat exchangers. For single-phase applications the majority of augmentation techniques focus on the disruption and destabilization of the thermal boundary layer, whereas, two-phase flow applications typically rely on heat transfer enhancers or surface modification to increase the boiling activity near the heat transfer surface. Unfortunately, the penalty associated with

* Corresponding author. Address: Dana Corporation, Thermal Products, Long Manufacturing Division, 656 Kerr Street, Oakville, Ont., Canada, L6K 3E4. Tel.: +1 905 631 5680; fax: +1 905 845 0685.
E-mail address: jim_cotton@longmfg.com (J. Cotton).

0017-9310/$ - see front matter © 2005 Elsevier Ltd. All rights reserved.
doi:10.1016/j.ijheatmasstransfer.2005.05.032

Nomenclature

A	area (m^2)
C_p	specific heat—constant pressure (J/kg K)
D	diameter (m)
E	electric field strength (V/m)
E_{hd}	EHD number
M_d	Masuda number
f	force density (N/m^2)
f''_e	electric force density (N/m^2)
F_e	Electric Froude number
Fr	Froude number
g	gravitational acceleration (m/s^2)
G	mass flux (kg/m^2s)
Gr	Grashof number
h	heat transfer coefficient (W/m^2 K)
h_L	stratified liquid level (m)
I	current (A)
k	thermal conductivity (W/m K)
L	length (m)
$\dot{m}$	mass flow rate (kg/s)
Nu	Nusselt number
P	pressure (Pa)
q	power (W)
q''	heat flux (W/m^2)
R	radius (m)
Re	Reynolds number
t	time (s)
T	temperature (°C)
u	velocity (m/s)
V_i	voltage applied to electrode (V)
We	Weber number
x	vapour quality

Greek symbols

ε_s	dielectric constant ($\varepsilon_s = \varepsilon/\varepsilon_0$)
ε	permittivity (N/V^2)
ε	permittivity of free space ($\varepsilon_0 = 8.854 \times 10^{-12}$ N/V^2)
μ	dynamic viscosity (kg/m s)
μ_c	ion mobility (m^2/V s)
μ	permeability (N/A^2)
ν	kinematic viscosity (m^2/s)
ρ	mass density (kg/m^3)
ρ_{ei}	charge density (C/m^3)
σ	standard deviation

Subscripts

0	vacuum or reference
b	bottom
h	hydraulic
i	local, or inner
in	inlet
l, L	liquid
o	outer or outlet
R	refrigerant
Sp	single-phase
S	surface
t	top
SAT	saturation state
V	vapour
W	water

conventional enhancement techniques is a significant increase in pressure drop. Among the novel enhancement techniques which do not involve a severe increase in pressure drop is a method commonly referred to as *electrohydrodynamics* (EHD). For two-phase flow applications, the electric field distribution and the difference in the specific dielectric constant, ε_s, of the two phases ($\varepsilon_L/\varepsilon_V \sim 10$), can contribute additional body forces not present in single-phase applications and may lead to a significant heat transfer enhancement. Both experimental and theoretical studies have shown that the resulting forces may lead to a reduction in the thermal boundary layer, increased convection, bubble or droplet migration and deformation, and interfacial instabilities or phase migration that can result in flow regime redistribution.

Previous works on EHD convective boiling have confirmed that EHD can significantly increase the heat transfer coefficients. However, comparison between these studies is difficult since the wide range of test section geometries and flow configurations lead to measurements that are system dependent. Horizontal tube-side flow boiling has been the focus of several investigations [1–8]. Although noting considerable heat transfer enhancement, the majority of these experiments also indicate that the level of augmentation can decrease with an increase in mass flux and inlet quality. The existence of an optimum enhancement has been attributed to the relative influence that the EHD forces and inertial forces have on determining the flow regime. At low qualities the EHD effects cause a flow regime redistribution which significantly influences the heat transfer. This is diminished as the inertial forces become the dominant forces that determine the flow pattern. In addition, depending on the mass flux, some studies have shown that the liquid extraction phenomena may promote early partial dry out which can have an unfavorable effect on the heat transfer [3,8].

Cotton et al. [7] and Bryan and Seyed-Yagoobi [9] proposed that the EHD augmentation of heat transfer during flow boiling is due to the redistribution of the

two-phase flow pattern created by liquid–vapour interfacial electric forces, in particular the dielectrophoretic force. However, without a quantitative measure of this force at the vapour–liquid interface only qualitative observations based on experimental trends and flow visualization studies could be performed. To contribute to this effort, the evaluation of the instantaneous static electric field distribution together with an accompanying order of magnitude assessment of the net EHD force acting on the flow have been performed in a recent investigation by Cotton et al. [1]. Using the forces predicted in that study this investigation presents an EHD two-phase flow pattern map, in annular geometries, using the Taitel and Dukler's [10] map as the foundation of a mechanistic transition criterion.

2. Electrohydrodynamic forces for flow boiling of Freon 134a

The application of an electric field in two-phase flow can contribute additional body forces within the bulk of a fluid as well as at the liquid/vapour interface. The electric force imposed on the flow field is traditionally represented by [11–13]

$$\bar{f}_e = \rho_{ei}\overline{E} - \frac{1}{2}E^2\nabla\varepsilon + \frac{1}{2}\nabla\left[\rho E^2\left(\frac{\partial\varepsilon}{\partial\rho}\right)_T\right] \tag{1}$$

Simply described, the three terms on the right-hand side of Eq. (1) represent the *electrophoretic*, *dielectrophoretic*, and *electrostrictive* components of the force, respectively. The physical significance of each term is summarized as follows:

(i) The *electrophoretic* force results from the net free charge within the fluid or injected from the electrodes. The interactions within the individual phases are typically associated with this component.
(ii) The *dielectrophoretic* force is a consequence of inhomogeneity or spatial change in the permittivity of the dielectric fluid due to non-uniform electric fields, temperature gradients, and phase differences.
(iii) The *electrostrictive* force is caused by inhomogeneous electric field strength and the variation in dielectric constant with temperature and density.

As discussed in detail in the following sections, the differences in the dielectric constant between the liquid and vapour, and therefore the dielectrophoretic effect, is the primary factor affecting the flow. In the present study, the difference was approximately an order of magnitude, $\varepsilon_l = 9.5$ for liquid compared to $\varepsilon_V = 1.09$ for vapour HFC-134a at the average saturation temperature 24 °C. A detailed discussion of the transport and electrical property data and correlations for HFC-134a is reported in [14]. The additional electric energy consumption due to the electric field is considered negligible when applied to a dielectric fluid, given the magnitude for conductivity in typical dielectrics is normally between 10^{-10} and $10^{-16}\,\Omega^{-1}\,m^{-1}$.

The equations of electrohydrodynamics, in spite of their complexity, may be resolved through a dimensional analysis which, as in classical theory, is a powerful procedure to elucidate flow behavior that cannot be rigorously calculated. The electric body force may be represented by two dimensionless EHD numbers [7,13];

$$E_{hd} = \frac{I_o L^3}{\rho_o \nu^2 \mu_c A}$$

the EHD number or conductive Rayleigh number (2)

$$M_d = \frac{\varepsilon_o E_o^2 T_o (\partial\varepsilon_s/\partial T)_\rho L^2}{2\rho_o \nu^2}$$

the Masuda number or dielectric Rayleigh number (3)

Using the analogy to free convective flows, the combined effects of electric and forced convection must be considered when $(E_{hd}/Re^2) \sim 1$ and/or $(M_d/Re^2) \sim 1$. If the inequalities $(E_{hd}/Re^2) \ll 1$ or $(M_d/Re^2) \ll 1$ are satisfied, electric convection effects may be neglected, and conversely, if $(E_{hd}/Re^2) \gg 1$ or $(M_d/Re^2) \gg 1$, forced convection effects may be neglected. This is exactly analogous to buoyancy driven flow and a similar argument may be made by comparing the EHD numbers to the Grashof number in the absence of forced convection. This order of magnitude analysis is useful in determining the range and extent to which EHD may influence the flow and must be identified to determine the voltage levels required to induce the migration of the liquid in order to affect heat transfer. Accordingly, the dimensionless groupings (E_{hd}/Re^2) and (M_d/Re^2) are plotted as a function of applied voltage in Figs. 1 and 2, respectively.

Considering the dimensionless analysis performed on other classical flows, such as natural convection, together with the previous investigations with EHD [13], it is expected that the inequality $E_{hd}/Re_l^2 \sim \geqslant 0.1$ is sufficient to define the minimum condition above which significant influences on the flow of liquid in the channel may be observed due to an electric field. Based on an order of magnitude comparison, the combined effects of electric induced flow and forced convection are represented by the shaded regions in Figs. 1 and 2. Fig. 1 indicates that for the conditions considered in this investigation E_{hd} is unlikely to play a role on a redis- tribution of the phases. Conversely, Fig. 2 shows that $M_d \sim Re_l^2$ so that the dielectric forces are significant.

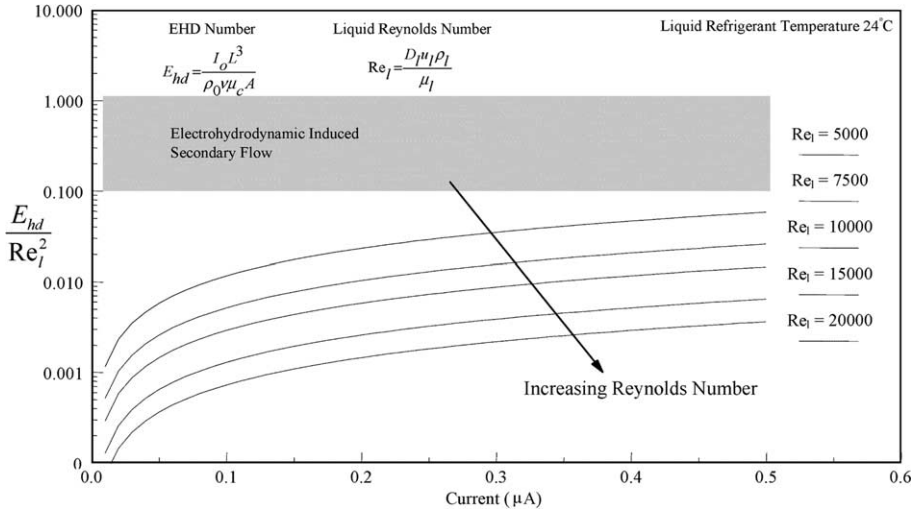

Fig. 1. The relationship between the EHD number and Reynolds number ratio as a function of current for the experimental arrangement. E_{hd} is calculated at 24 °C [7].

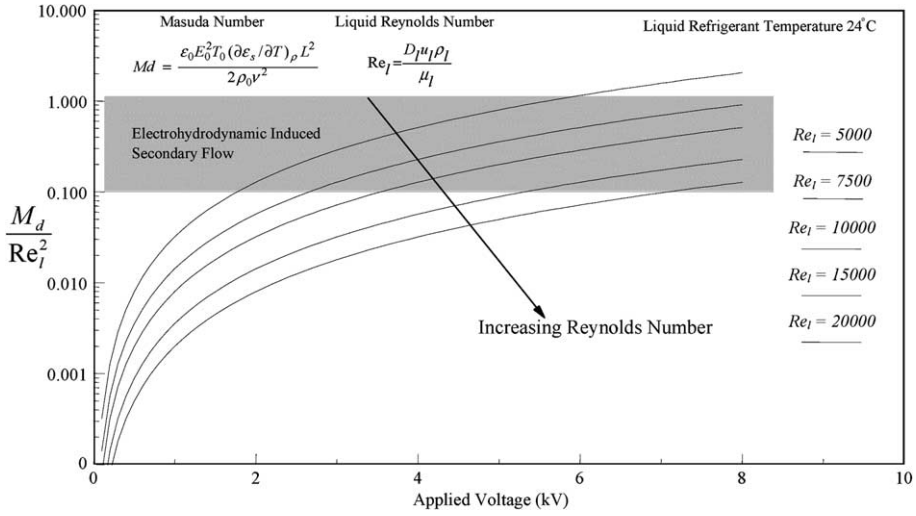

Fig. 2. The relationship between the Masuda number and Reynolds number ratio as a function of applied voltage for the experimental arrangement. M_d is calculated at 24 °C [7].

Fig. 2 indicates that the influence of the dielectrophoretic and electrostrictive components increase with increased voltage (i.e., electric field strength) and decrease with Reynolds number. The dimensionless ratio suggests that the EHD component will dominate when the flow is extremely slow, well into the laminar regime, with an applied voltage greater than about 6.0 kV. In addition, the dimensional analysis also suggests that for $Re_l > 20{,}000$ or $V_i \geqslant \sim 2$ kV the flow condition will be determined primarily by forced convection and EHD will not significantly affect the liquid flow such that flow redistribution due to electrohydrodynamic forces becomes unlikely.

3. Flow pattern map with electrohydrodynamic forces

As discussed in Cotton et al. [1,7] the most pronounced effect of the EHD force density can be realized in the region where the flow regime changes from stratified to intermittent or annular. This phase redistribution depends upon how significant the EHD force

density components are with respect to the fluid momentum and the quality. To determine this relation the numerical electrical force acting on the interface determined by Cotton et al. [1] was incorporated into the classical Kelvin–Helmholtz instability analysis performed by Taitel and Dukler [10], later extended by Steiner [15] and modified in this work to accommodate annular geometries.

In the present model, the assumption used by Taitel and Dukler [10] and Steiner [15] for plain tubes has been adopted for an annular geometry with EHD. The basic principle is that all flow regimes are manifested due to a perturbation from the horizontal stratified flow regime. Suppose that a small perturbation occurs on the interface of a stratified flow in an annular channel where a high voltage is applied to the inner tube. The vapour flowing over the protrusion will accelerate, causing a drop in the vapour pressure and thus producing suction on the protrusion that will cause it to grow unless the suction is more than offset by the surface tension and gravitational forces acting downward on the protrusion. Contributing to the growth of the protrusion are the electrically induced interfacial forces acting against gravity as discussed qualitatively by Cotton et al. [1]. Therefore, the instability analysis must include the effects of inertia, energy storage in the gravitational field and surface tension effects, as well as the electrical interactions with the interface. Based on the extended Taitel and Dukler [10] analysis proposed by Steiner [15] the condition for the growth of the protrusion is:

$$F_e^2\left(\frac{\overline{A}_V^3}{\overline{A}^2\cdot d\overline{A}_L/d\bar{h}_L}\left[\frac{\pi^2}{25\bar{h}_L^2}\left(\frac{Fr}{We}\right)_L\right]+1\right)\geqslant 1 \tag{4}$$

where F_e is the electric Froude number given by Chang [16,17]

$$F_e=\frac{xG}{(\rho_V[(\rho_L-\rho_V)D_o g-f_e'])^{1/2}} \tag{5}$$

As proposed by Cotton et al. [1] in order to understand the basic character of the possible additional instabilities, the interfacial force, f_e'', is considered in a situation of greatest possible simplicity, that is uniform fields and plane geometry to perform an order of magnitude analysis such that the relative forces may be compared. As indicated by Melcher [18], certain phenomena, often associated with nonuniform fields, are accounted for by the dynamics of a surface acted on by a uniform field. Based on this reasoning, the analysis of the interfacial force on a charge-free interface, explored by previous investigators for two immiscible fluids separated by a plane interface between two parallel rigid boundaries was employed [16,18–22]. The fluids are presumed inviscid, incompressible, perfect dielectrics and it has been assumed that the motion of the fluids does not disturb the source of the electric field.

For the polarization-charge interaction where the interface does not support free-charge, the charge density, ρ_{ei}, in the electrophoretic component not only vanishes everywhere in the bulk, but at the interface as well. Melcher [18] derived the interfacial force by means of a direct dynamic analysis, as follows:

$$f_e''=\frac{\varepsilon_L(\varepsilon_L-\varepsilon_V)^2}{\varepsilon_V(\varepsilon_L+\varepsilon_V)}\varepsilon_o E_L^2=\frac{\varepsilon_V(\varepsilon_L-\varepsilon_V)^2}{\varepsilon_L(\varepsilon_L+\varepsilon_V)}\varepsilon_o E_V^2 \tag{6}$$

where E_L and E_V are the electric field in the liquid and vapour phases at the interface. These electrical stresses tend to cause the dielectric having the higher permittivity to move into the space occupied by the other [20]. Based on the electric field distribution observed through the finite element analysis of a stratified liquid–vapour arrangement with concentric electrodes this migration is vertically upwards against gravity at all liquid levels [1]. Thus, converting Eq. (4) to the graphical representation as suggested by Kattan et al. [23] the transition from stratified flow in EHD annulus systems is given by

$$G\geqslant\left(\frac{\overline{A}_V^3[(\rho_L-\rho_V)D_o g-f_e'']}{\overline{A}^2\cdot d\overline{A}_L/d\bar{h}_L}\left[\frac{\pi^2}{25\bar{h}_L^2}\left(\frac{Fr}{We}\right)_L\right]+1\right)^{\frac{1}{2}}\cdot\frac{1}{x} \tag{7}$$

For comparison purposes, the flow regime transition criterion with and without an applied voltage is presented in Fig. 3, using Eq. (7) with the interfacial electrical forces developed by Melcher [18]. The electric field is assumed to be uniformly distributed at a strength equivalent to the maximum electric field strength that could develop if liquid refrigerant were to fill the entire annular gap to demonstrate an order of magnitude effect (i.e., $E_{Sp}=V_i/(R_i\ln(R_o/R_i))$) with an electrode voltage of $V_i=8.0$ kV at a system temperature of 24 °C. As predicted through the static force balance [1], the interfacial electrical force reduced the required inertia generated suction pressure for transition to occur at a given liquid level as shown in Fig. 3. The degree to which

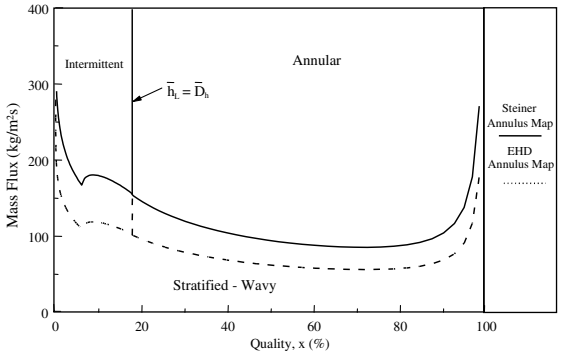

Fig. 3. Proposed flow pattern map for an annular channel under the influence of an 8.0 kV DC voltage potential.

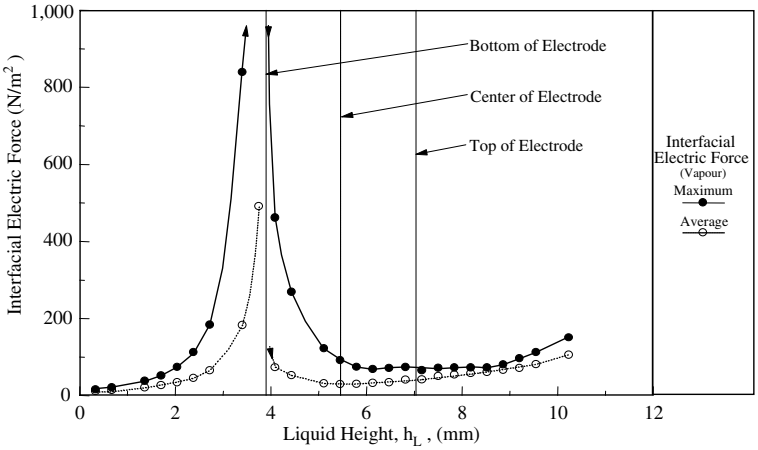

Fig. 4. Average and maximum interfacial electric force as a function of the liquid height.

the transition is augmented depends strongly on the liquid level, however it must be stated that this analysis is presented in its simplest form such that the basic character of the effect of an electric field may be developed. In reality the electric field for a stratified flow in an annular geometry is far from uniform [1]. The non-uniformities in the electric field distribution calculated numerically shows that the one-dimensional procedure developed by Taitel and Dukler [10] and extended by Chang [17] to incorporate electric fields is not comprehensive enough to describe the coupling of flow regimes and an electric field for the present problem. However, phenomena associated with nonuniform fields are often accounted for by the dynamics of a surface stressed by a uniform field [18]. If this is true for the dynamic action of electrical effects on flow patterns, the problem is to determine how a certain nonuniform field may be transformed into a uniform field.

Based on the static system model of Cotton et al. [1], as the liquid height is increased, the forces acting on the interface increase. This is better depicted when the predicted average and maximum interfacial electric forces are plotted against the liquid height in Fig. 4. As Fig. 4 shows, the interfacial force increases with the increasing liquid level for a significant portion of the channel area (more than 85%). Further, in the range where the interfacial force is decreasing, the magnitude of the maximum force is above the energy stored in the gravitational field. Therefore, if a protrusion were to exist on the interface, a localized electric force would develop, at least in the maximum strength region, that would be self-propagating. Although this is a time dependent local phenomenon, due to interfacial tension effects the surrounding liquid would be "dragged" upwards with the fluid into the region of the maximum field strength. Considering the self-propagating nature of a perturbation in the vicinity of the maximum electric field, the corresponding maximum interfacial electrical force is conjectured to be the appropriate force to represent the uniform field in the one-dimensional instability analysis.

4. The refrigerant test facility for experimental validations

Fig. 5 shows a schematic of the experimental test facility used to study the flow pattern in EHD flow boiling [8]. It is a closed loop charged with the refrigerant HFC-134a as the working fluid. The main components of the loop are: the pump, electrically heated sections, hot water heated section, condenser, pressurizer, test section and various measuring devices. The test section used was a concentric tube single-pass counter-current flow heat exchanger 1.5 m in length, with a stainless tube 1.8 m in length, 12.7 ± 0.5 mm outside diameter and 10.92 ± 0.5 mm inside diameter, which contained the two-phase refrigerant mixture (Fig. 6). The heating jacket used water as the working fluid. The outer tube was 1.5 m in length, with an inner diameter of 20.8 mm and an outside diameter of 26.7 mm. The inner tube was equipped with thermocouples at six axial locations, 250 mm apart, top and bottom, for tube wall surface temperature measurement. The 0.5 mm thermocouples were inserted in 25 mm × 0.5 mm grooves, cut to a depth of 0.5 mm along the length of the test section to measure the local surface temperature. The axial water temperature distribution was measured at five top and bottom locations in addition to both inlet and outlet.

To avoid both interference in the temperature measurements due to the applied high voltage and hardware and software cold junction compensation errors, an ice bath was constructed to the specifications outlined in ASTM STP 470 (1970). The bath was assumed isothermal at a temperature of 0.01 °C, as the standard speci-

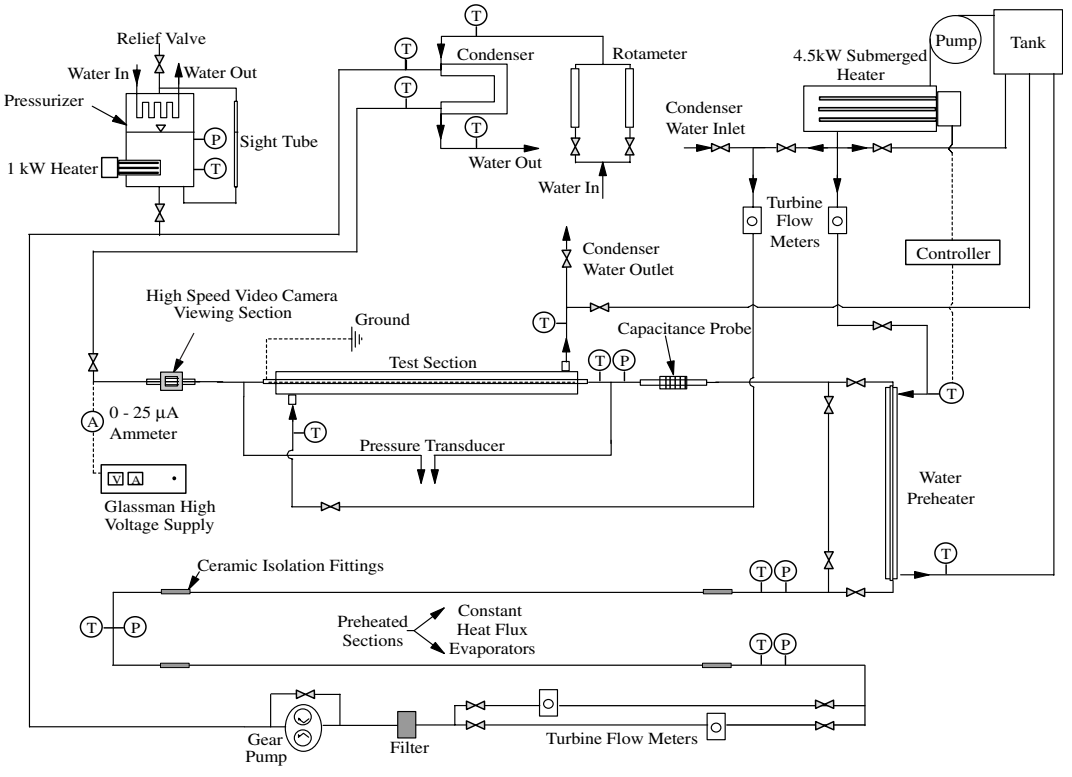

Fig. 5. Experimental test facility.

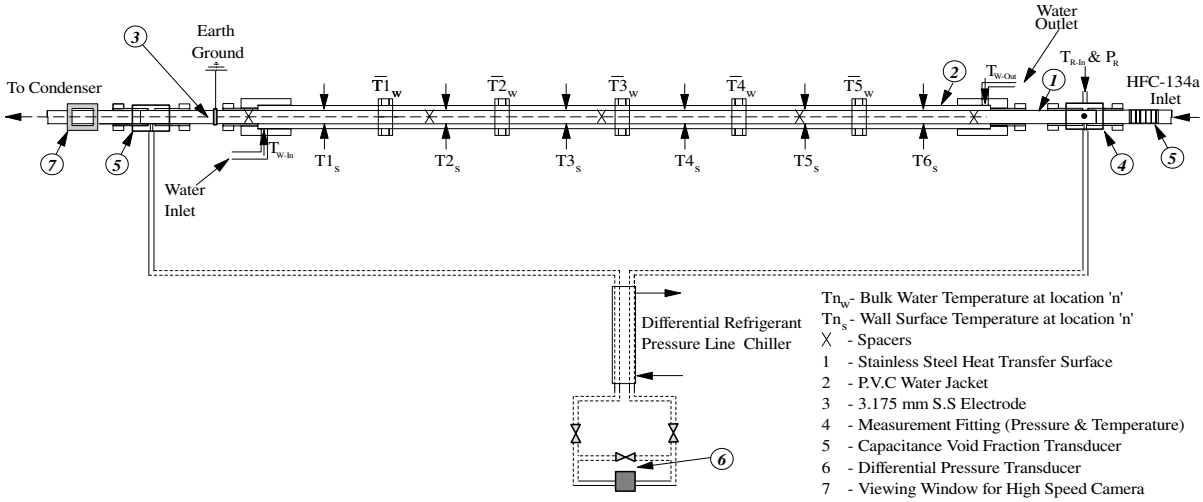

Fig. 6. Schematic diagram of test section.

fied. The total emf was then converted to a temperature using individual system calibration curves for each thermocouple. The calibrated accuracy was within ±0.1 °C. Validation experiments were performed to ensure that the measured temperature was within the calibrated accuracy and to confirm that the voltage applied did not affect the measured signal. It was found that in regions were the EHD effect was suppressed by inertial flow dominance the applied voltage had no effect on the measured temperatures. Also the temperature measurements were qualitatively confirmed by comparing the outlet flow pattern observed by high speed photography

to the temperature differences of the top and bottom surface thermocouples 12.5 mm from the exit of the heat exchanger.

The coaxial electrode was a stainless steel 3.175 mm rod. The annular gap was maintained by five nonconducting spacers strategically placed to minimize interference with the surface temperature thermocouples. The high voltage was supplied by a DC power supply (Glassman Series EL model EL30R1.5), with reversible polarity up to 30 kV and a maximum current output of 1.5 mA. The pressure drop across the test section was measured by a Validyne differential pressure transducer with a 34.47 kPa (5 psi) diaphragm. High speed video imagining of the flow regime at the exit of the test section was performed at 1000 f/s by a Kodak EktaPro EM 1000 Imager.

In order to assess the effect of EHD on the two-phase heat transfer both average heat transfer coefficient of the discretized area of the test section and the overall heat transfer coefficient was determined. The calculation of discretized average heat transfer coefficients was based on energy balance on the water side at any two axial positions along the test section. For the present analysis, the top and bottom water temperatures were averaged and values of heat transfer rates were determined for 0.5 m lengths. It was then assumed that the heat flux was circumferentially uniform over a 0.5 m long length.

$$q_{i\to i+2} = \dot{m}_{\mathrm{W}} c_{p\mathrm{W}} (T_{\mathrm{W}_{i+2}} - T_{\mathrm{W}_{\mathrm{i}}}) \tag{8}$$

The inner tube was divided into 12 sections, 0.25 m in length, 6 to represent the top and 6 the bottom halves of the tube.

With the axial heat transfer rates determined, the average heat transfer coefficient of the top and bottom portions of the tube was determined by assuming that the two local measurements of surface temperature were approximately equivalent to the temperature of the 0.25 m section for the bottom and top half of the channel, respectively. The top and bottom heat transfer coefficients are

$$h_{i_{\mathrm{t}}} = \frac{q_{i\to i+1}}{4A(T_{i-S_{\mathrm{t}}} - T_{\mathrm{SAT}})}, \quad h_{i_{\mathrm{b}}} = \frac{q_{i\to i+1}}{4A(T_{i-S_{\mathrm{b}}} - T_{\mathrm{SAT}})} \tag{9}$$

where the area is $A = 1/2\pi L D_{\mathrm{i}}$ ($L = 0.25$ m, $D_{\mathrm{i}} = 10.92$ mm). The overall heat transfer coefficient is then determined by averaging the sectioned bottom and top heat transfer coefficients

$$\bar{h}_{\mathrm{i}} = \frac{1}{12} \sum_{1-\mathrm{t,b}}^{6-\mathrm{t,b}} h_{i_{\mathrm{t,b}}} \tag{10}$$

Full details of the test section, electrode spacers, voltage supply, data acquisition system and experimental procedure, error analysis and validation protocol is provided in [14]. The associated measurement error and calculation uncertainty of the data processed is calculated using the root mean sum square method. The maximum experimental uncertainties for the primary performance indicator are: heat flux [±10%], Reynolds number [±3%], quality [±6%], heat transfer coefficient [±14%] and Nusselt number [±15%].

5. Influence of a DC electric field on the heat transfer and pressure drop

Vaporization enhancement is to be expected if a stratified two-phase flow were to redistributed to "wet" parts of the channel that were previously "dry", for example, a change to annular flow, or if a quantity of liquid in contact with the tube is extracted which in turn acts to "thins" the thermal boundary layer. Conversely, if the electric field established acts to create an attraction force, drawing the liquid from the surface of the tube such that dry out occurs, then a reduction in heat transfer may be observed. To describe this effect, an example of a sectional analysis of the heat exchanger is presented in Fig. 7 for the following conditions: $Re_{\mathrm{l}} = 3500$, $x_{\mathrm{in}} = 0\%$, and $q'' = 10.2\ \mathrm{kW/m^2}$ at different voltage levels for the top and bottom halves of the tube. The overall performance results show an enhancement of nearly 100%, whereas locally the effects range from enhancement by as much 2000% to suppression in heat transfer of 40% over the no EHD condition.

As will be discussed, for the conditions presented in Fig. 7 the measurement of the local surface temperatures suggests that the dominant flow pattern is likely stratified wavy, which explains the significant difference in heat transfer coefficients from the top to the bottom. When the applied voltage is increased, there is an increase in local heat transfer over the circumference of the tube. This may be explained by considering the resultant forces acting on the liquid–vapour interface. As the high voltage is applied, the dielectrophoretic force can create protrusions on the interface producing a significantly more disturbed flow with the potential for more frequent and larger amplitude waves. The vapour flowing over the protrusions accelerates, reducing the vapour pressure which enhances the upward force causing a wave to grow unless it is more than offset by the downward gravitational and surface tension forces. As the protrusion grows the electric field distribution in the vapour phase changes so that the attractive force on the liquid increases, further accelerating the wave upwards. If the combined flow effects are strong enough, a flow regime transition will occur changing the stratified liquid to either intermittent or annular. Regardless, the result is a reduction in the liquid thickness on the bottom of the tube and a wetting of the top, which will increase the rate of heat transfer around the tube as a consequence. As heat is added to the system at a voltage level above approximately $V_{\mathrm{i}} = 4.0$ kV, the quality

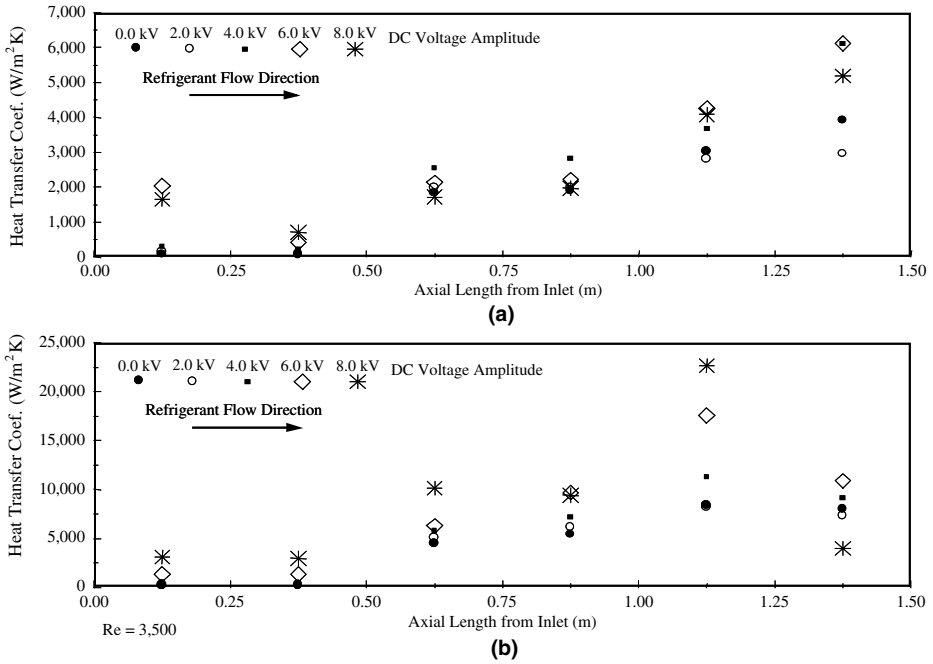

Fig. 7. Average heat transfer coefficients at discretized segments of the heat exchanger with increasing applied voltage. (a) Heat transfer coefficients along the top portion of the tube and (b) heat transfer coefficients along the bottom portion of the tube.

increases and the rate of heat transfer becomes more symmetric. Here the flow is believed to be slug or annular flow. In the case of annular flow, the highest electric field is near the electrode in the vapour core so that the liquid will be extracted from the wetted surface by the resultant attractive force. As reported by Norris et al. [8], this results in a regime of intermittent dry out on the bottom surface thereby reducing the overall heat transfer.

Considering the global EHD effect on the heat exchanger can provide insight into the mechanisms that may affect performance. The overall heat transfer enhancement results of the experimental investigation are presented in Figs. 8–10 together with the corresponding time averaged pressure drop measurements. All results are presented in terms of dimensionless variables based on the Laplace electric field at the inner electrode (for a single-phase fluid) as the reference value and the properties of saturated liquid [14]. The results are presented in terms of average Nusselt number, $Nu_{D_h} = \bar{h}_i D_h/k_l$, and overall pressure drop as a function of the Masuda number (Eq. (3)), the liquid Reynolds number, $Re_{D_h} = \dot{m}D_h/A_i\mu_l$, and inlet quality of different heat flux levels. The results show that:

- The rate of heat transfer increases with increasing Masuda number.
- As the Reynolds number increases above 7000, the inertia forces tend to suppress the influences of the electric field.
- The degree of augmentation highly depends on the initial flow pattern as shown by the non-monotonic behavior of the inlet quality.
- The pressure drop increases with increasing applied voltage regardless of whether heat transfer enhancement is observed. This is primarily due to the establishment of unstable flow patterns created by the continuously changing electric field which are prone to increased momentum interaction of the liquid and vapour, hence pressure losses along the length of the tube.

These brief examples shows the complexity of EHD induced flow augmentation for a given set of conditions and identifies the importance of flow pattern recognition in any attempt to identify the mechanisms involved under the influence of EHD flow and heat transfer augmentation.

6. Experimental validation of modified flow pattern map

For conditions studied in Fig. 7, the proposed EHD flow pattern map (Fig. 11), provides and indication of the flow pattern expected for EHD flow boiling. Fig. 11 suggests that for the specific case of a saturated liquid entering the heated section with a constant mass flux of $G \sim 100\ \mathrm{kg/m^2s}$, the flow is prone to be in the

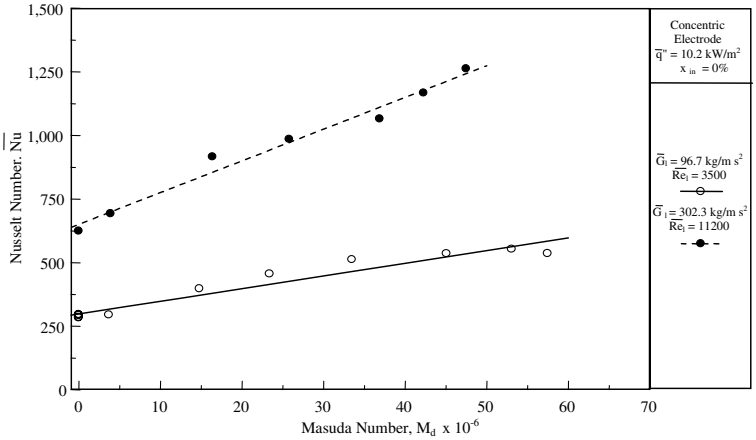

(a) Nusselt Number vs. Masuda Number

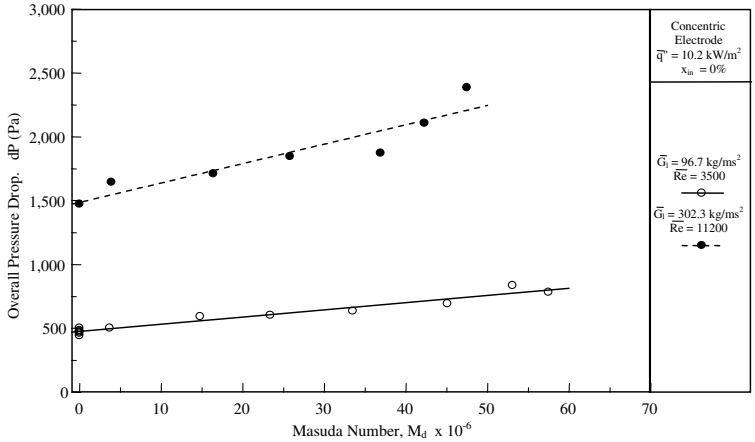

(b) Overall Pressure Drop vs. Masuda Number

Fig. 8. The effect of Masuda number on: (a) the average Nusselt number and (b) the overall pressure drop, for fixed heat flux (10.2 kW/m^2) and inlet quality (0%) for various Reynolds numbers.

stratified regime for qualities greater than $x = 0\%$ and less than approximately $x \sim 50\%$ in the absence of an electric field. However, for the inlet conditions the quality must be in the range: $0 < x \geqslant \sim 12\%$ for stratified flow to exist upon application of an 8.0 kV electric field. The transition quality is expected to increase with voltage levels below this extreme. As the heat flux was held constant for all voltage levels considered, the outlet quality is also constant at $x_{out} \sim 40\%$. Therefore, in the absence of an electric field, the prediction of the flow regime is stratified flow along the majority of the channel. Conversely, for an 8.0 kV electric field the flow is believed to experience two transitions, one from stratified wavy flow to intermittent flow at the approximate location where $x \sim 12\%$ and a second above approximately $x \sim 20\%$ where the flow is expected to be annular. As the proposed fully developed flow regime map does not account for momentum transfer between the phases, the effects of acceleration and the nonuniform electric force acting on the interface, these boundaries only present a reasonable qualitative estimation.

The outlet flow pattern observed from the experiments at 8.0 kV voltage is also presented in Fig. 11. The proposed transition boundary correctly identifies the transition from stratified flow for all but four conditions investigated. Further it is apparent that the EHD effect seems to have a minimal influence on the proposed transition criterion from intermittent to annular flow. As the figure shows, the effect of the body force is not as dominant at high qualities as suggested in Fig. 3 but increases as the liquid level increases, or alternatively, as the quality decreases. This continues until the quality exceeds approximately 40% and the interfacial electric force exceeds the combined effect of gravity and surface tension. At this level, it is assumed that the liquid will be drawn increasingly upwards until these restraining forces are no longer exceeded resulting in an annular flow regime or possibly an unstable entrained droplet

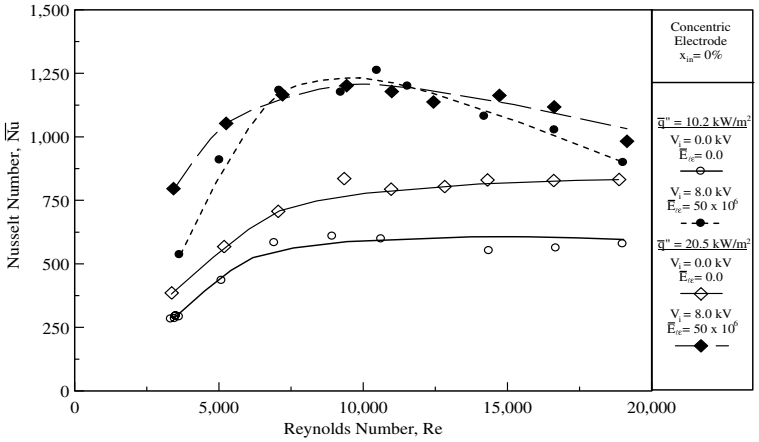

(a) Nusselt Number vs. Reynolds Number

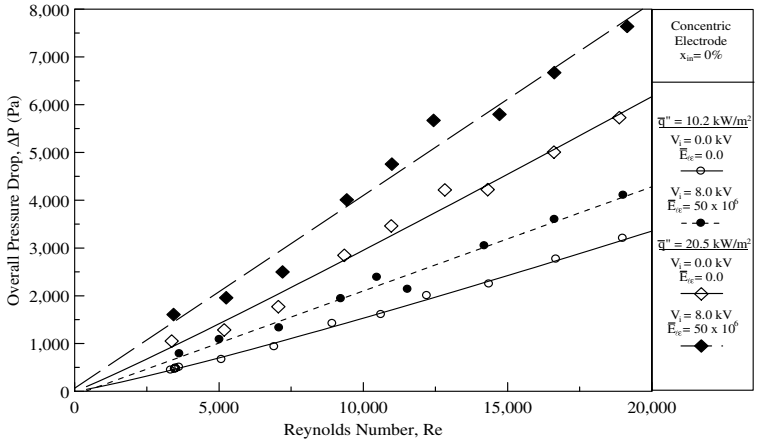

(b) Overall Pressure Drop vs. Reynolds Number

Fig. 9. The effect of Reynolds number on: (a) the average Nusselt number and (b) the overall pressure drop, with and without applied voltage for a fixed inlet quality of 0% at different heat flux levels.

flow pattern. This zone is represented by the cross-hatched line. As the quality decreases further, the mass flux must be increased for transition to occur due to the increased surface tension effects which reduce the impact of the electric field. This trend continues until the electrical force again exceeds the restraining forces, creating a state whereby transition is presumed to occur at negligible mass flow levels.

7. Heat transfer analysis

Fig. 12a shows the axial profile of the time-averaged superheat temperatures, $(\overline{T}_s - \overline{T}_{SAT})$, at the top and bottom of the test section tube along the heated test section for the 0 kV, 4 kV and 8 kV test cases, respectively at the same flow conditions considered in Fig. 7, ($G = 100$ kg/m^2 s, $q'' = 10$ kW/m^2, $x_{in} = 0\%$). Fig. 12b shows the associated standard deviation of the surface temperature fluctuations, determined according to

$$\sigma = \left[\frac{1}{n}\sum_{i=1}^{n}(T_i - \overline{T}_s)^2\right]^{1/2} \tag{11}$$

A higher standard deviation indicates that the temperature at that point fluctuates more about the corresponding time-averaged value over the course of the sampling period. Standard deviations in the range of ±0.05–0.08 °C may be assumed to represent a constant temperature reading since this variation in temperature is on the order typical of white noise fluctuation. Even though the heat capacity of the tube tends to filter high frequency components of the fluctuations, the surface temperature and standard deviation profiles provide enough information that reasonable inferences can be made about the flow pattern at any axial location along the tube [14].

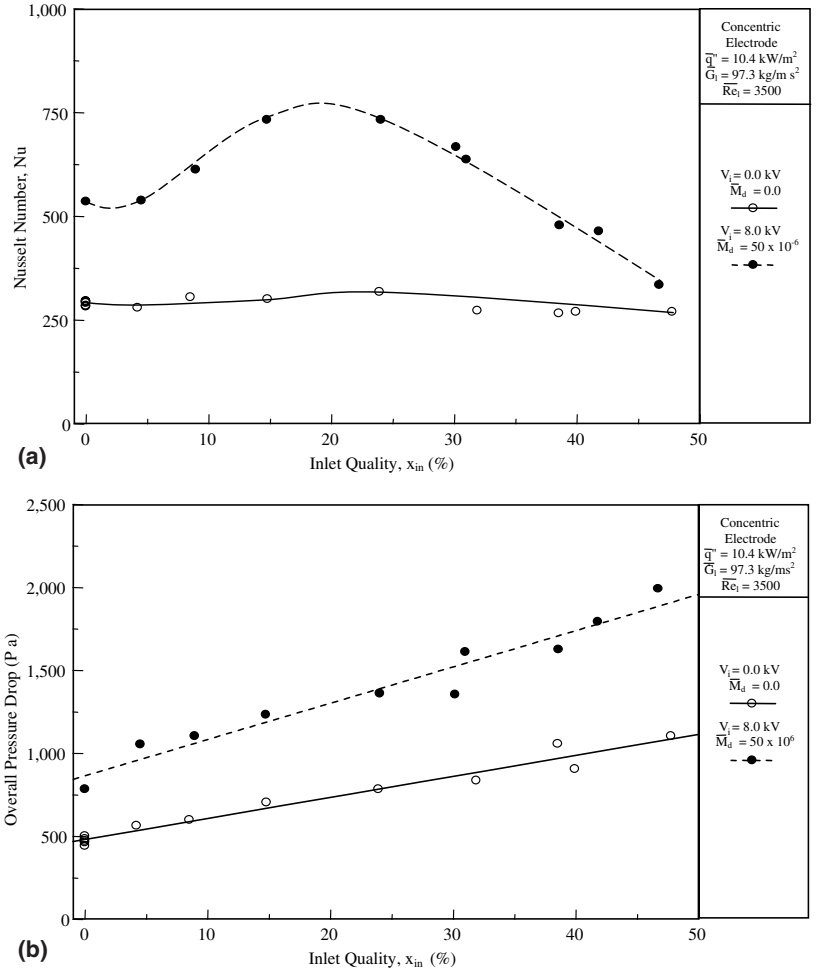

Fig. 10. The effect of inlet quality on: (a) the average Nusselt number and (b) the overall pressure drop, with and without applied voltage at for fixed heat flux (10.4 kW/m^2) and $Re_l = 3500$.

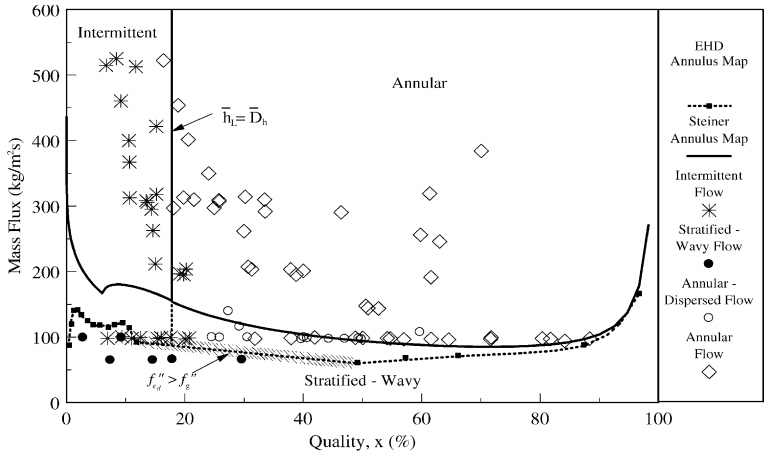

Fig. 11. Outlet EHD flow pattern data (8.0 kV) compared against the proposed EHD flow pattern map applying the maximum interfacial body force determined through a finite element analysis.

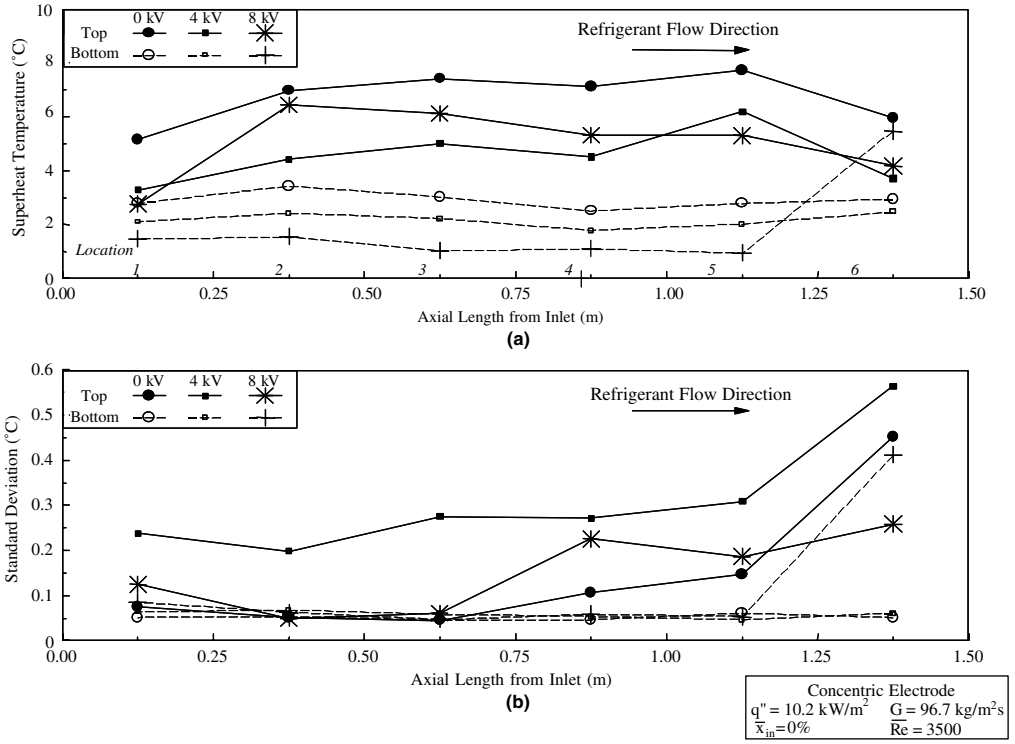

Fig. 12. (a) Time-averaged surface superheat and (b) standard deviation profiles for increasing DC applied voltage levels.

7.1. Convective flow boiling flow pattern without and applied voltage

Fig. 12a shows that for $V_i = 0.0$ kV, the magnitudes of the bottom superheat do not vary significantly along the tube length. This, coupled with the fact that Fig. 12b shows that the surface temperature can be considered constant at each axial location, suggests that the bottom surface is continuously wetted along its entire length. Conversely, Fig. 12 indicates that the top surface superheat and standard deviation change significantly along the length of the test section implying axial variation of the flow regime.

At thermocouple location 1, Fig. 12a shows that the average superheat of the top surface is more than 2 °C higher than the bottom indicating flow and/or thermal stratification inside the tube. At the same location Fig. 12b shows that the standard deviation of the top wall temperature is slightly higher than that of the bottom signifying that the top surface is intermittently wetted while the bottom surface is wetted continually. Considering the measured superheat temperature is sufficient to produce some nucleation, the greater standard deviation of the top surface is attributed to bubble ebullition around the circumference of the tube, migration of bubbles upwards due to buoyancy and the flow of vapour plugs as bubbles coalesce.

Fig. 12a indicates that the temperature between locations 2 and 5 is essentially uniform and about 2 °C higher than location 1. The rise in surface temperature means that the local heat transfer coefficient has decreased which can be realized if the top surface is no longer "wetted". This, together with the small temperature fluctuations for both the top and bottom measurements indicated in Fig. 12b implies that the likely flow regime at these locations is stratified wavy as is predicted by the flow pattern map given in Fig. 11. Further examination of Fig. 12b also reveals that at locations 4 and 5, noticeable disturbances exist compared to the previous locations causing the standard deviation to increase. This is likely due to droplet entrainment and subsequent impingement on the top of the channel resulting from increased instability on the liquid vapour interface since the vapour velocity increases with increasing quality. Finally, the trend of slightly increasing temperature on the upper surface may be accredited to the counterflow configuration of the test section. Conversely, the slightly decreasing bottom wall temperature is likely due to a decreasing thermal resistance associated with a decreasing stratified liquid layer thickness. Inconsistencies in these trends may be a result of the pressure drop along the channel, reducing the refrigerant's saturation temperature, although this did not exceed 0.4 °C during this investigation.

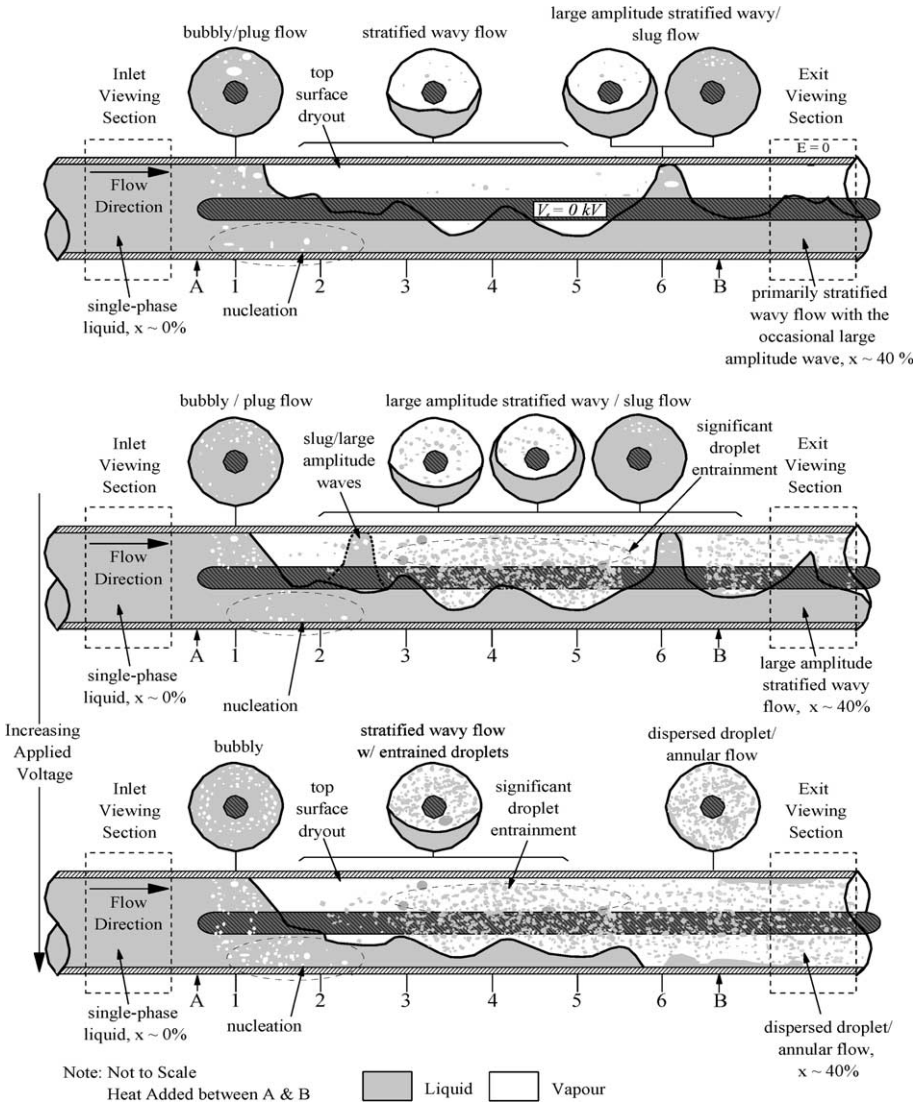

Fig. 13. Proposed reconstructed flow pattern from surface temperature measurements and inlet and outlet flow observations for increasing DC voltage levels ($G = 100\ \mathrm{kg/m^2\,s}$, $q'' = 10\ \mathrm{kW/m^2}$, and $x_{in} = 0\%$).

The final surface temperature measurements are 12.5 cm upstream from the exit of the heated section. Here, Fig. 12b reveals that the standard deviation increases dramatically indicating that the top surface is alternately dried and rewetted, presumably by slugs bridging the channel gap, significant droplet entrainment in the vapour or the intermittent wetting of the surface due to "climbing" of liquid around the circumference of the tube. Since the bottom surface seems to be wetted, the likely flow regime near the exit is stratified wavy/slug flow. This is confirmed by the flow pattern map given in Fig. 11 as well as by examination of high speed video imaging at the viewing windows just upstream of the heated section [14]. The schematic of the proposed flow pattern reconstruction in the absence of an electric field is presented in Fig. 13.

7.2. Convective boiling flow pattern under applied voltage

The proposed dimensional analysis ($M_d \sim Re_l^2$) predicts that $V_i = 4.0$ kV appears to be the threshold of the EHD effect (Fig. 7). The profound influence on the heat transfer is emphasized by a notable decrease in the top and bottom wall temperatures as compared with the 0 kV case illustrated in Fig. 12a together with a significant increase in the standard deviation of the top surface temperature over the entire length of the test

section. The bottom superheat measurements for $V_i = 4.0$ kV shows that once again, the bottom surface is wetted along the entire length. With regards to the top surface temperature, the fluctuations at location 1 have increased enough that it is believed that the boiling dynamics may have intensified due to the influences affecting bubble detachment and coalescence. The temperature fluctuations at locations 2–6 give rise to standard deviation values from 0.2 °C increasing to nearly 0.6 °C and are indicative of a surface that is alternately dried and rewetted [14]. This is presumably due to the action of slug flow, significant droplet entrainment or the intermittent wetting due to climbing of liquid around the circumference of the tube. Since the overall heat flux is constant regardless of the applied voltage, the liquid must be taken from the previously stratified liquid layer. As the refrigerant moves downstream and the local quality increases, the liquid layer at the bottom becomes thinner which increases the degree to which the bottom surface is cooled thus allowing the temperature of the wall to be lower. A second effect is that as the applied voltage level is increased the interfacial electric force increases, enhancing the momentum suction pressure effect which attracts the liquid towards the upper part of the channel. With decreasing liquid layer thickness, interfacial waves are expected to increase due to the increase in vapour velocity and increased nonuniformity of the electric field as more liquid is drawn upwards and entrained into the vapour core. By entraining from the stratified layer upwards against gravity, through the influence of the interfacial electric forces, the thinner liquid layer increases the heat transfer coefficient along the bottom surface which in turn decreases the wall superheat. Further, redistributing the liquid and vapour to wet the upper portions of the channel that were previously dry, increases the heat transfer coefficient along the top surface which accounts for the decreases in the wall superheat. The schematic of the proposed flow pattern reconstruction in the presence of an applied voltage of $V_i = 4.0$ kV is presented in Fig. 13.

Fig. 12a and b clearly show differences with a more intense electric field, $V_i = 8.0$ kV. At location 1 the top and bottom superheat temperatures have decreased by ~2 °C while the fluctuations have increased only slightly over the $V_i = 0$ kV condition. The likely causes of these effects are that the electric field increases the number of bubbles by breaking up large bubbles and decreasing the bubble detachment diameter, thereby resulting in the creation of more turbulence and interfacial area. Here, the resulting flow pattern is postulated to be a more concentrated, uniformly dispersed bubble flow.

The large increase in the top surface temperature in conjunction with the negligible fluctuations observed for both the top and bottom temperature readings between stations 1 and 2 are indicative of a change in flow regime from dispersed bubble flow to stratified flow. However, the upper surface temperatures between locations 3 and 5 are observed to continually decrease. This at first seems counter intuitive since the temperature is expected to increase downstream whenever the flow configuration is unchanged, owing to the countercurrent nature of the heat exchanger. However, considering the increased intensity of the electric field, the rate of liquid entrainment into the vapour core will also increase substantially. As a consequence of this there will be considerable droplet impingement on the otherwise dry top surface. The observed decrease in the top surface temperature is thus speculated to be a result of the increased heat transfer coefficient associated with the additional cooling effect of droplet impingement [14]. As the measurements indicate, this effect should intensify as the flow develops down stream, further reducing the surface temperature, based on the argument posed earlier that interfacial waves are expected to increase due to the increase in vapour velocity and increased nonuniformity and intensity of the electric field as more liquid is drawn upwards and entrained into the vapour core. Finally, at location 6 a considerable deviation from the previous two tests (#59, #63) is apparent as shown in Fig. 12a and b. At this location, the wall temperature of the bottom surface has increased to a point where it is close to the temperature of the top surface. Further, Fig. 12b indicates that the standard deviation of the bottom temperature of the channel is considerably higher than the bottom temperature measurements upstream of that location. Due to the similarity between the top and bottom temperature measurements, the flow influences are assumed to be similar. Here, both the top and bottom tube surfaces are intermittently dried due to the extraction of liquid into the vapour core, which reduces the rate of heat transfer. With the support of high speed video imaging this regime was identified as a transitional regime between annular and highly dispersed droplet flow. The schematic of the proposed flow pattern reconstruction in the presence of an applied voltage of $V_i = 8.0$ kV is presented in Fig. 13.

8. Pressure drop analysis

Fig. 14a presents the overall pressure drop variation across the heat exchanger for $V_i = 0.0$ kV. For this condition, the mean overall pressure drop is 480 Pa with a 60 Pa standard deviation. Compared to the adiabatic experiments conducted by Cotton et al. [24], fluctuations of this magnitude are rather small for a two-phase system and are typical of non-periodic flow regimes such as bubbly, annular, stratified wavy or mist flow. This is consistent with the inferences made from the temperature measurements and flow pattern map that the dominant flow regime may be stratified wavy. The transient pressure drop trace for $V_i = 4.0$ kV, shown in Fig. 14b,

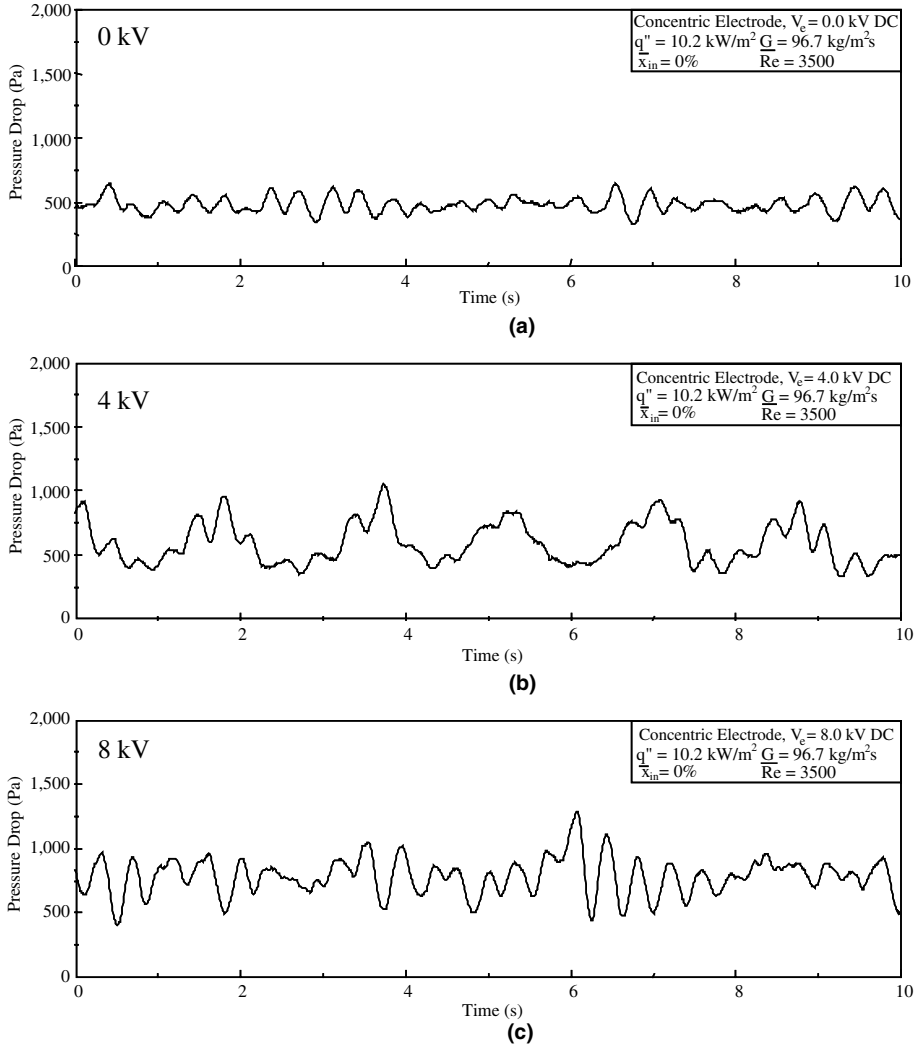

Fig. 14. Time trace of pressure drop for increasing applied voltage levels.

exhibits 5–10 considerable surges in pressure over the 10 s data acquisition period, similar to pressure drop fluctuations observed in a slug type flow. Consequently, with the application of an electric field the mean overall pressure drop and standard deviation has increased to 590 ± 160 Pa due to this more unstable flow regime. Fig. 14c indicates that for $V_i = 8.0$ kV the pressure differential is approximately 800 Pa with a standard deviation of 150 Pa and does not maintain a repetitive structure like the former test, $V_i = 4.0$ kV. At $V_i = 8.0$ kV, the increase in pressure drop is a function of the establishment of unstable flow patterns prone to increase momentum interaction, i.e., entrained droplet flow, and the less structured nature of the instantaneous values are believed to be due to the numerous flow pattern transitions that seem to occur axially along the length of the channel.

9. Conclusions

A dimensional analysis has shown that the electrohydrodynamic forces become significant, and EHD may influence a forced convective flow, when the ratio of the Masuda number is of the same order of magnitude as the square of the liquid Reynolds number, $M_d \sim Re_l^2$. The flow boiling experiments have provided evidence that when the proposed dimensionless criterion is satisfied, EHD body forces have a strong influence on the liquid-phase and consequently the flow pattern within the channel. This flow redistribution is the primary mechanism affecting the increase in pressure drop and the augmentation or even suppression of heat transfer. This work has also shown the importance of determining the flow regime if accurate methods of estimating flow boiling heat transfer rates are to be developed for

EHD enhanced convective boiling. To accomplish this the electric field distribution analysis presented by Cotton et al. [1] was used to determine the interfacial electric forces which were subsequently introduced into a modified flow pattern map to account for the electric field effect on the transition boundaries between stratified and annular or intermittent flows. Combining this flow pattern map and electric field analysis with the experimental overall parametric study, the axial flow patterns progression was reconstructed to explain the pressure drop increase and heat transfer augmentation observed. In general it was found that when the flow redistribution wet parts of the channel that were previously dry (i.e., changed stratified flow to annular) or thinned the thermal boundary layer by extracting liquid in contact with the tube, vaporization enhancement occurred.

Acknowledgements

This work is partially supported by Dana Corporation, Long Manufacturing Division (JSC, MS, AJR), The Natural Science and Engineering Research Council of Canada (JSC) and ASHRAE (JSC, MS).

References

[1] J.S. Cotton, D. Brocilo, J.S. Chang, M. Shoukri, T. Smith-Pollard, Numerical simulation of electric field distributions in electrohydrodynamic two-phase flow regimes, IEEE Trans. Dielectrics Electrical Insulation 10 (1) (2003) 37–50.

[2] A. Yabe, T. Taketani, H. Maki, K. Takahashi, Y. Nakadai, Experimental study of electrohydrodynamically (EHD) enhanced evaporator for non-azeotropic mixtures, ASHRAE Trans. 98 (2) (1992) 455–461.

[3] A. Singh, M.M. Ohadi, S. Dessiatoun, W. Chu, In-tube boiling heat transfer enhancement of R-123 using the EHD technique, ASHRAE Trans. 100 (2) (1994) 818–825.

[4] M. Salehi, M.M. Ohadi, S. Dessiatoun, EHD-enhanced convective boiling of R-134a in grooved channels—application to compact heat exchangers, ASME J. Heat Transfer 119 (1995) 805–809.

[5] M. Salehi, M.M. Ohadi, S. Dessiatoun, The applicability of the EHD technique for convective boiling of refrigerant blends-experiments with R-404A, ASHRAE Trans. 102 (1) (1996) 839–844.

[6] J. Seyed-Yagoobi, J.T. Hardesty, P. Raghupathi, J.E. Bryan, Experimental study of electrohydrodynamically augmented pool boiling heat transfer on smooth and enhanced tubes, J. Electrostat. 40/41 (1997) 597–602.

[7] J.S. Cotton, M. Shoukri, J.S. Chang, T. Smith-Pollard, Electrohydrodynamic (EHD) flow and convective boiling augmentation in single-component horizontal annular channels, 2000 International Mechanical Engineering Congress and Exposition, HTD-366-4, 2000, pp. 177–184.

[8] C. Norris, J.S. Cotton, M. Shoukri, J.S. Chang, T. Smith-Pollard, Electrohydrodynamic effects on flow redistribution and convective boiling in horizontal concentric tubes, ASHRAE Trans. 105 (1) (1999) 222–236.

[9] J.E. Bryan, J. Seyed-Yagoobi, Influence of flow regime, heat flux, and mass flux on electrohydrodynamically enhanced convective boiling, J. Heat Trans. 123 (2001) 335–367.

[10] Y. Taitel, A.E. Dukler, A model for predicting flow regime transition in horizontal and near horizontal gas–liquid flow, AIChE J. 22 (1976) 47–55.

[11] W. Panofsky, M. Phillips, Classical Electricity and Magnetism, second ed., Addison-Wesley, Pub. Co., Reading, MA, 1962.

[12] L.D. Laudau, E.M. Lifshitz, Electrodynamics of Continuous Media, Pergamon, NewYork, 1963.

[13] J.S. Chang, A. Watson, Electromagnetic hydrodynamics, IEEE Trans. Dielectrics Electrical Insulation 1 (5) (1994) 871–895.

[14] J.S. Cotton, Mechanisms of electrohydrodynamic (EHD) flow and heat transfer in horizontal convective boiling channels, Ph.D Thesis, McMaster University, Hamilton, Canada, 2000.

[15] D. Steiner, Heat transfer to boiling saturated liquids, VDI-Wärmeatlas (VDI Heat Atlas), in: Verein Deutscher Ingenieure, (Ed.), VDI-Gessellschaft Verfahrenstechnik und Chemieingenieurwesen (GCV) [Translator: J.W. Fullarton], Düsseldorf, Germany, 1993.

[16] J.S. Chang, Two-phase flow in electrohydrodynamics, in: A. Castellanos (Ed.), Part V, Electrohdyrodynamics, International Centre for Mechanical Sciences Courses and Lectures No. 380, Springer, New York, 1998.

[17] J.S. Chang, Stratified gas–liquid two-phase electrohydrodynamics in horizontal pipe flow, IEEE Trans. Ind. Appl. 25 (2) (1989) 241–247.

[18] J.R. Melcher, Field-Coupled Surface Waves: A Comparative Study of Surface-Coupled Electrohydrodynamic and Magnetohydrodynamic Systems, MIT Press, Cambridge, MA, 1963.

[19] K. Brunner, J.S. Chang, Flow regime transition under electric fields in horizontal two-phase flow, in: Proc.15th IEEE Ind. Appl. Soc. Conf., 1980, pp. 1042–1047.

[20] K.C. Kao, Some electromechanical effects on dielectrics, British J. Appl. Phys. 12 (November) (1961) 629–632.

[21] R.L. Johnson, Effect of an electric field on boiling heat transfer, AIAAJ 6 (August) (1968) 1456–1460.

[22] W.J. Duffin, Electricity and Magnetism, McGraw-Hill, Toronto, 1973.

[23] N. Kattan, J.R. Thome, D. Favrat, Flow boiling in horizontal tubes, part 1: Development of a diabatic two-phase flow pattern map, ASME J. Heat Transfer 120 (February) (1998) 140–147.

[24] J.S. Cotton, A. Abdul-Razzak, M. Shoukri, M. Richter, Pressure drop during two-phase flow of refrigerant R-134a in a horizontal pipe, in: CSME Symp. Hamilton, vol. 1, 1996, pp. 34–41.